

# Utilizing co-designed compliance for designing multi-articular robotics

**Abstract**—We investigated using co-design for optimizing mono- and biarticular compliant actuators inspired by human musculature. Six bio-inspired compliant actuators were defined that were co-designed in four different configurations, applied to a 3-DoF leg model. The results showed that, compared with a fully actuated series-elastic actuator configuration, co-designed compliance showed significant reduction in energy consumption of around 80% on average, with a biarticular configuration performing best with a 90% reduction, which is contributed to its use of energy transfer between the biarticulated joints. The bio-inspired actuators used in multiple configurations showed its co-designed parameters converged to similar results, and were comparable to what was found in literature, showing that co-design could be used to design mono- and biarticular compliant actuation.

**Index Terms**—optimal control, CasADi, biarticulation, compliant actuation, trajectory optimization, co-design.

## I. INTRODUCTION

Over the last decades, robotics have evolved from being single-task machines to being more dynamic problem solvers. With improvements in computation and actuation, allowing for more computationally challenging control in smaller robotics, the emphasis on good design becomes more important. One source of inspiration is mimicking biology, attempting to translate muscle function and topology into actuator concepts, based on the assumption that the human musculature has evolved to minimize energy consumption. Muscle function is often expressed with the three-element muscle model [1], which consists of the active part expressing the contraction and energy storage in elasticity [2], and the passive part expressed as the general elasticity of the tissue. This shows the muscle acting as a non-linear progressive elastic elements, capable of storing energy, which is used by the body to optimize movement. It is also used to increase apparent stiffness in joints with antagonistic muscle pairs, resulting in more precise movement and control [3] as well as biarticulation; a muscle that spans multiple joints. This allows for the transfer of mechanical energy between the joints, which allows proximal muscles to assist deficient distal muscles [4].

Using muscles as inspiration we look into compliant actuation, which allows us to mimic muscle function by copying the active branch from the three-element muscle model, with the actuator controlling the tension. Compliant actuators are widely used due to safety [5], [6] and capacity of storing energy [7]–[10]. This also extends to biarticulated compliance, which also shows to improve control effort [10], [11] and in simulations shows better performance than purely mono-articulated models [8], [9], [12].

Including mono- and biarticulation introduces a new complexity to design, with several methods for determining actuator parameters. Instead of grid search [7], or optimizing parameters to compensate for gravity [13], we can utilize co-design to optimize parameters, a methodology where design parameters and control are optimized in parallel. There are various different implementations; most often trajectory optimization (TO) is used, in which the co-design parameters are included [7]. Another approach is bi-level, splitting the design and control optimization into two separate loops. The control loop often uses TO, with the co-design using a different optimization methods like genetic algorithms [14], stochastic programming [15] or motion planning algorithms [16].

The aim of this work is to investigate co-design of mono- and biarticulated actuation parameters to create better designs. We obtain results through simulation studies with a simplified leg model combined with different configurations of actuators inspired by human musculature. The approach to compliant actuators is inspired by Roozing et al. [8], [13], [17], [18], which allows for flexible implementation of muscle-like actuators. For the simulation, a TO problem including co-design parameters is defined consisting of moving the leg through different orientations whilst preserving stability. This work contributes the by:

- defining a TO problem in which the leg model is tasked with moving to 10 waypoints in variable time. The leg model is controlled by five different configurations, one baseline and four bio-inspired, resulting in five trajectories optimized for energy efficiency. The four bio-inspired configurations use additional mono- and biarticulated actuators inspired by human musculature, the parameters of which are optimized through co-design;
- comparing the results of co-designing mono-articular and especially biarticular actuators, which reproduced energy efficiency as seen in aforementioned works and shows the effectiveness of co-design as a tool for designing mono- and biarticular actuators for robotics.

The work will first define the models and configurations used in TO in section II. Section III will contain an explanation of the TO problem that contains our co-design problem and method of improving convergence. In section IV we will define the TO problem and its variables used and show the results. Section V will discuss the findings and shortcomings of the results and model. We conclude the work with section VI.

## II. MODELLING

The modelling is divided into two parts; the leg model and the actuator model. The leg model is modelled as effort-in, flow-out and the actuator model is modelled as flow-in, effort-out. This allows us to formulate different combinations of actuators to apply to the leg model.

### A. Leg model

The leg model is modelled after a human leg in the sagittal plane, shown in fig. 1. It consists of three links  $l_1, l_2, l_3$  originating from the ankle, knee and hip joint  $\theta_1, \theta_2, \theta_3$  with torques  $\tau_1, \tau_2, \tau_3$ , and are damped by viscous friction with coefficients  $d_1, d_2, d_3$ . The links are modelled as 2D rigid bodies with  $m_1, m_2, m_3$  defining the link masses placed at the center of each link with rotational inertia  $J_1, J_2, J_3$ . At the top of  $l_3$  load mass  $m_4$  is located with rotational inertia  $J_4$ . We define the foot with mass  $m_0$  to calculate stability parameters, explained in section III-B, and has no effect on the dynamics. It is considered fixed to floor and defines the the Base of Support (BoS) with  $x_h, x_t$ , denoting the  $x$ -position of the heel and toes w.r.t. the ankle. With states  $\mathbf{q} = [\theta_1, \theta_2, \theta_3]^T$  the rigid body dynamics are:

$$\ddot{\mathbf{q}} = M(\mathbf{q})^{-1} [\boldsymbol{\tau} + \mathbf{G}(\mathbf{q}) - D\dot{\mathbf{q}}], \quad (1)$$

with damping matrix  $D = \text{diag}[d_1, d_2, d_3]$  denotes joint friction, and  $\mathbf{G}(\mathbf{q})$  denotes the generalized gravitational torque:

$$\mathbf{G}(\mathbf{q}) = J_g(\mathbf{q})^T \mathbf{G}_c, \quad (2)$$

with gravitation vector  $\mathbf{G}_c$  containing the gravitational forces caused by link and load mass, and  $J(\mathbf{q})$  denotes the system Jacobian. We ignore Coriolis and centripetal forces. The generalized inertia matrix is defined as:

$$M(\mathbf{q}) = J(\mathbf{q})^T M_c J(\mathbf{q}), \quad (3)$$

with nominal inertia matrix  $M_c$  defined as a diagonal matrix containing link mass, load mass and rotational inertia.

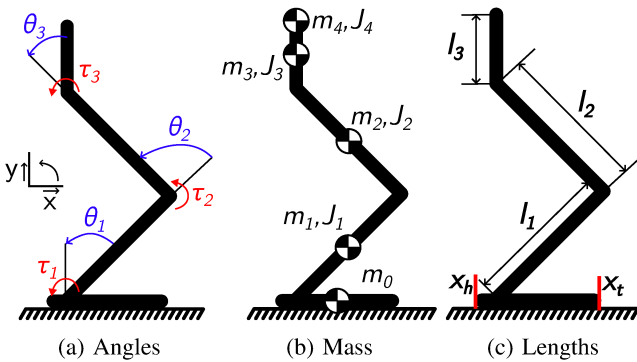


Fig. 1: Leg model

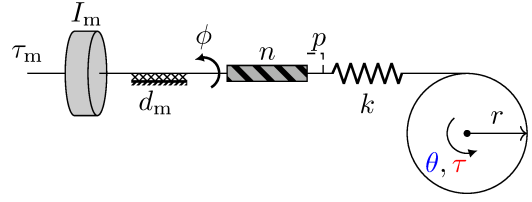


Fig. 2: Pretension actuator model

### B. Actuator model

Our actuator model is based on the formulation described by Roozing et al. [8], [18], where an actuator model is defined to describe compliant actuation for both mono- and biarticular implementations, which control the pretension position of the compliant element. The model is shown in fig. 2 and we express the dynamics of a singular general actuator with state  $p$  as follows:

$$n^2 I_m \ddot{p} + n^2 d_m \dot{p} + k \Delta = n \tau_m, \quad (4)$$

with rotor inertia  $I_m$ , viscous friction coefficient  $d_m$ , ball screw transmission ratio  $n$ , spring stiffness  $k$  and the elongation of the spring given by:

$$\Delta = p + \mathbf{r} \cdot \mathbf{q}, \quad (5)$$

with adjustable pretension position  $p$  and pulley radius vector  $\mathbf{r}$ . This vector is defined as  $\mathbf{r} = [r_1, r_2, r_3]^T$  corresponding to the joint angles  $\mathbf{q} = [\theta_1, \theta_2, \theta_3]^T$  with the sign of  $r_i$  indicating the direction of  $\theta_i$  that increases the elongation. Using this model, we define two different actuator types, referred to as SEA and MA for the rest of this work, using  $[\cdot]_{\text{SEA}}$  and  $[\cdot]_{\text{MA}}$  to improve readability. MA represents Muscle-inspired Actuator, and is used for both mono- and biarticular implementations with high stiffness meant for storing energy. The SEA represents a Series Elastic Actuator which applies its torque to a joint without pulley  $\mathbf{r}$  and therefore unlike MA, SEA do not slack, so the generated torques are:

$$\tau_{\text{MA}} = \begin{cases} -[\mathbf{r}^T k \Delta]_{\text{MA}}, & \text{if } \Delta_{\text{MA}} > 0 \\ 0, & \text{if } \Delta_{\text{MA}} \leq 0 \end{cases}, \quad (6)$$

$$\tau_{\text{SEA}} = -[\mathbf{r}^T k \Delta]_{\text{SEA}}. \quad (7)$$

$\mathbf{r}$  determines if an actuator is SEA or MA and mono- or biarticular. For a SEA applied to joint  $i$  we define  $r_i = -1$  and obtain the following:

$$\Delta_{\text{SEA}} = p_{\text{SEA}} - \theta_i, \quad (8)$$

$$\tau_{\text{SEA}} = -[\mathbf{t}^T k \Delta]_{\text{SEA}}, \quad (9)$$

which also requires us to redefine  $p_{\text{SEA}}$  as an angle,  $n_{\text{SEA}}$  as the gearbox transmission ratio and  $k_{\text{SEA}}$  as torsional stiffness, which differ in units and order of magnitude but follow the same dynamics equation (4). The implementation of a mono-

articular MA on joint  $i$  and biarticular MA on joint  $i$  and  $j$  gives us the following:

$$\boldsymbol{\tau}_{\text{mono}} = -\mathbf{r}^T k_{\text{mono}} (p_{\text{mono}} + r_i \theta_i), \quad (10)$$

$$\boldsymbol{\tau}_{\text{bi}} = \begin{bmatrix} \tau_{\text{bi}_i} = -r_i k_{\text{bi}} (p_{\text{bi}} + r_i \theta_i + r_j \theta_j) \\ \tau_{\text{bi}_j} = -r_j k_{\text{bi}} (p_{\text{bi}} + r_i \theta_i + r_j \theta_j) \\ 0 \quad \forall \notin \{i, j\} \end{bmatrix}^T, \quad (11)$$

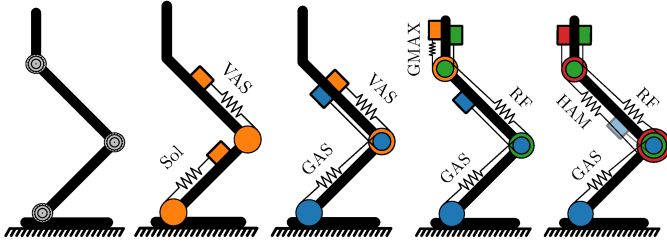
and we note that  $\boldsymbol{\tau}_{\text{SEA}}$ ,  $\boldsymbol{\tau}_{\text{mono}}$  and  $\boldsymbol{\tau}_{\text{bi}}$  contain zeros corresponding with angles they do not actuate. This allows us to sum all actuator torques, for  $N_{\text{act}}$  number of actuators, this is:

$$\boldsymbol{\tau} = \sum_{a=1}^{N_{\text{act}}} (-\mathbf{r}_a^T k_a \Delta_a), \quad (12)$$

which gives us our input vector for our leg model (1).

### C. Actuator configurations

For the simulations, five different configurations are used. All five consist of at least three SEA, each placed on one of the three joints. These configurations are shown in fig. 3, and have color-coded MAs to make the reading of results easier. All mono-articulated MAs are colored orange and biarticular MAs will be defined when introduced. The actuators do not add mass to the system, which creates a comparison purely based on performance.



(a) Config 0 (b) Config 1 (c) Config 2 (d) Config 3 (e) Config 4

Fig. 3: Schematics of the five different configurations

1) *Configuration 0; SEA only (fig. 3a)*: The first configuration will be done as a baseline measurement, showing fully actuated performance using solely SEAs.

2) *Configuration 1; Mono-compliance (Figure 3b)*: This configuration add two mono-articulated MA; the Soleus (SOL) to the ankle joint and the Vastus Lateralis (VAS) to the knee joint. These joints require the highest torques in this direction for movements like bending forwards or squatting.

3) *Configuration 2; Single Biarticulation (fig. 3c)*: The first biarticulated configurations adds two MAs; the VAS and the Gastrocnemius (GAS, in blue), which provides the ankle and the knee with positive torque. In humans, the GAS is responsible for running and jumping movements, and should be able to transfer energy from the VAS.

4) *Configuration 3; Double Biarticulation (fig. 3d)*: To measure the impact of multiple biarticulated actuators, this configuration adds three MAs; the GAS, the Rectus Femoris (RF, in green) and the Gluteus Maximus (GMAX) extending possible energy transfer to include the hip. The GMAX acts

as antagonist to the RF to see if it assists distal joints by transferring energy for movements like squatting.

5) *Configuration 4; Triple Biarticulation (fig. 3e)*: The last configuration adds three MAs; the GAS, the RF and the Hamstrings (HAM, in red). This configuration only has biarticular MAs, with the RF and HAM as an antagonistic muscle pair, to see if it improves controllability like in humans.

As mentioned before, each configuration is actuated with 3 SEAs:  $\mathbf{r}_{\text{SEA}}^1 = [-1, 0, 0]^T$ ,  $\mathbf{r}_{\text{SEA}}^2 = [0, -1, 0]^T$  and  $\mathbf{r}_{\text{SEA}}^3 = [0, 0, -1]^T$ . The MAs are defined as follows;

$$\mathbf{r}^{\text{SOL}} = [-r_1^{\text{SOL}}, 0, 0]^T \quad (13)$$

$$\mathbf{r}^{\text{VAS}} = [0, r_2^{\text{VAS}}, 0]^T \quad (14)$$

$$\mathbf{r}^{\text{GMAX}} = [0, 0, -r_3^{\text{GMAX}}]^T \quad (15)$$

$$\mathbf{r}^{\text{GAS}} = [-r_1^{\text{GAS}}, -r_2^{\text{GAS}}, 0]^T \quad (16)$$

$$\mathbf{r}^{\text{RF}} = [0, r_2^{\text{RF}}, r_3^{\text{RF}}]^T \quad (17)$$

$$\mathbf{r}^{\text{HAM}} = [0, -r_2^{\text{HAM}}, -r_3^{\text{HAM}}]^T \quad (18)$$

### III. TRAJECTORY OPTIMIZATION

As our simulations consist of several TO problems, we first express our co-design problem in the form of TO. This is formulated as follows:

$$\min_{\mathbf{x}, \mathbf{u}, T, \gamma} J(\mathbf{x}, \mathbf{u}, T, \gamma), \quad (19)$$

$$\text{s.t. } \dot{\mathbf{x}}(t) = \mathbf{f}(\mathbf{x}(t), \mathbf{u}(t), \gamma) \quad \forall t \in [0, T], \quad (20)$$

$$\mathbf{h}(\mathbf{x}(t), \mathbf{u}(t), T, \gamma) \leq 0 \quad \forall t \in [0, T], \quad (21)$$

$$\mathbf{g}(\mathbf{x}(0), \mathbf{x}(T), T, \gamma) \leq 0, \quad (22)$$

where we minimize cost function (19). This cost function is subjected to the system dynamics (20), path constraints (21) and boundary constraints (22). The cost function can be expressed as:

$$J(\mathbf{x}, \mathbf{u}, T, \gamma) = J_{\text{bound}}(\mathbf{x}(0), \mathbf{x}(T), T, \gamma) \quad (23)$$

$$+ \int_0^T J_{\text{path}}(\mathbf{x}(t), \mathbf{u}(t), T, \gamma) dt, \quad (24)$$

which consists of a boundary cost and a path cost. In our co-design problem, state vector  $\mathbf{x}(t) = [\mathbf{q}, \mathbf{p}, \dot{\mathbf{q}}, \dot{\mathbf{p}}]$  contains leg model states  $[\mathbf{q}, \dot{\mathbf{q}}]$  and the vector of all actuator states  $[\mathbf{p}, \dot{\mathbf{p}}]$ , input vector  $\mathbf{u}(t) = \boldsymbol{\tau}_m$  contains motor torque of all actuators.  $\mathbf{x}(t)$ ,  $\mathbf{u}(t)$ , final time  $T$  and co-design parameters  $\gamma$  are the decision variables that will be adjusted to minimize the cost function. For configuration 0, that does not apply co-design, our TO simplifies to only having  $(\mathbf{x}(t), \mathbf{u}(t), T)$  as decision variables.

#### A. Sequence of tasks

With the generalized expression of co-design, we formulate a sequence of tasks. Given  $N_t$  tasks, we obtain  $N_t$  co-design problems in series, visualized in fig. 4. This results in the following cost:

$$\min_{\{\mathbf{x}_i, \mathbf{u}_i, T_i\}, \gamma} \sum_{i=1}^{N_t} J(\mathbf{x}_i, \mathbf{u}_i, T_i, \gamma), \quad (25)$$

where all tasks use  $\gamma$  and are subject to the same system dynamics (20) and path constraints (21). We can also define the following boundary constraints that couple the tasks:

$$\mathbf{x}_1(0) = \mathbf{x}_{\text{init}}, \quad (26)$$

$$\begin{cases} \mathbf{x}_2(0) = \mathbf{x}_1(T_1) \\ \mathbf{u}_2(0) = \mathbf{u}_1(T_1) \end{cases}, \quad (27)$$

$$\vdots \quad (28)$$

$$\begin{cases} \mathbf{x}_{N_t}(0) = \mathbf{x}_{N_t-1}(T_{N_t-1}) \\ \mathbf{u}_{N_t}(0) = \mathbf{u}_{N_t-1}(T_{N_t-1}) \end{cases}, \quad (29)$$

$$\mathbf{x}_{N_t}(T_{N_t}) = \mathbf{x}_{\text{final}}, \quad (30)$$

which connects the tasks forming a sequence, creating the complete TO problem.

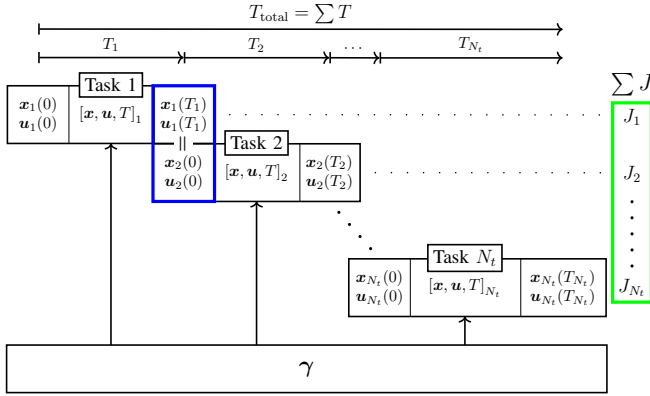


Fig. 4: Co-design split up into  $N_t$  sub-problems, solved in series with global co-design parameters  $\gamma$ .

## B. Cost function and constraints

To ensure our results resemble realistic trajectories and inputs, we apply hard (in)equality constraints, and adapt our cost function to include soft constraints. Soft constraints generally improve convergence whilst hard constraints are often necessary for forcing behavior.

1) *Cost function*: The cost function is often formulated in a way that minimizes effort as a path cost, including several soft constraints. Path cost is often defined by minimizing the required force squared [15], [19]. Although effective for TO, co-design requires us to include actuator performance into the effort. Therefore, co-design problems often choose to minimize the required power of the actuation [7], [8], [14], as adding this as a path constraint also minimizes energy consumption. For a configuration with  $N_{\text{act}}$  number of actuators, we obtain the following cost:

$$J_{\text{Power}} = \sum_{i=1}^{N_{\text{act}}} P_i(\mathbf{x}(t), \mathbf{u}(t), \gamma)^+, \quad (31)$$

where  $P_i^+$  defines the cost consists only of positive power, assuming our actuators are not able to recover power. This is approximated using a tanh function to preserve a continuous

derivative. We define the power consumption of actuator  $P_i$  as follows:

$$P_i(\mathbf{x}(t), \mathbf{u}(t), \gamma) = P_i^{\text{work}}(t) + P_i^{\text{loss}}(t), \quad (32)$$

$$P_i^{\text{work}}(t) = n_i u_i(t) \dot{\phi}_i(t), \quad (33)$$

$$P_i^{\text{loss}}(t) = \kappa_i^T u_i^2(t), \quad (34)$$

with  $\kappa_i^T$  defined as the torque constant of each motor. From preliminary testing we found that  $J_{\text{Power}}$  fails when  $-P_i^{\text{work}}(t) > P_i^{\text{loss}}(t)$ , turning  $P_i(\mathbf{x}(t), \mathbf{u}(t), \gamma)$  negative which has no cost attached, which presented oscillating behaviour in  $\Delta$  (5), requiring the following cost:

$$J_{\Delta} = \sum_{i=1}^{N_{\text{act}}} (\dot{p}_i + \mathbf{r}_i \cdot \dot{\mathbf{q}})^2, \quad (35)$$

which is squared to prevent negative cost. We finalize by defining a cost on the Zero-Moment Point (ZMP) of the model, responsible for keeping the leg model stable. The ZMP is based on a simplified cart-table model [20], and the cost is defined as follows:

$$J_{\text{ZMP}} = e^{\beta(x_{\text{heel}} - x_{\text{ZMP}})} + e^{\beta(x_{\text{ZMP}} - x_{\text{toes}})}, \quad (36)$$

$$x_{\text{ZMP}} = x_{\text{CoM}} + \frac{y_{\text{CoM}}}{y_{\text{CoM}} - g} x_{\text{CoM}}^{\ddot{\cdot}}, \quad (37)$$

$$(38)$$

where  $g = 9.81 \text{ m/s}^2$  denotes the gravitational constant and the following coordinates in reference frame fig. 1; the ZMP position  $x_{\text{ZMP}}$ , Base of Support (BoS)  $x_{\text{heel}}$  and  $x_{\text{toes}}$  and Center of Mass (CoM)  $x_{\text{CoM}}$ ,  $y_{\text{CoM}}$ . We combine path costs, obtaining:

$$J_{\text{path}} = \sum_{i=1}^{N_t} [w_P J_P]_i + [w_{\Delta} J_{\Delta}]_i + [w_{\text{ZMP}} J_{\text{ZMP}}]_i, \quad (39)$$

where  $w$  denotes the weighing factor used for obtaining results. We define our boundary cost as:

$$J_{\text{bound}} = w_T \sum_{i=1}^{N_t} T_i, \quad (40)$$

where we sum all task times in to obtain total time  $T_{\text{total}}$ , which is included into the cost function to force the configuration to complete its tasks within appropriate time, and does not spend too much unnecessary time in energy efficient orientations.

2) *Constraints*: In addition to the boundary constraints set for setting the tasks in sequence (III-A), we add the following boundary and path constraints, defined as follows:

$$T > 0, \quad (41)$$

$$T_{\text{total}} \leq T_{\text{max}}, \quad (42)$$

$$\mathbf{q}_{\text{min}} \leq \mathbf{q}(t) \leq \mathbf{q}_{\text{max}} \quad \forall t \in [0, T], \quad (43)$$

$$\Delta_{\text{MA}}(t) > 0 \quad \forall t \in [0, T], \quad (44)$$

$$x_{\text{ZMP}}^{\text{min}} \leq x_{\text{ZMP}}(t) \leq x_{\text{ZMP}}^{\text{max}} \quad \forall t \in [0, T], \quad (45)$$

$$\gamma_{\text{min}} \leq \gamma \leq \gamma_{\text{max}}, \quad (46)$$

which constrains task time to be positive and total time to be within acceptable limits. It sets limits to the leg joint angles, to realize physical constraints. As mentioned in eq. (6), we force MAs to only generate force under tension. The ZMP is constrained to keep its cost function from approaching infinity and the co-design parameters should optimize within an acceptable range.

### C. Collocation methods

Given the continuous dynamics, we use a collocation method to discretize our problem and be able to numerically solve using a computer. We use a direct collocation method which, as explained by Kelly [19], creates an approximation of our continuous dynamics using polynomial splines. The accuracy of this approximation mainly depends on the number of segments, with the trade-off of increased computation time. We use the 2nd order Hermite-Simpson collocation method proposed by Moreno-Martín et al. [21], which differentiates first and second order variables and allocates matching order splines for better performance. We implement this using CasADi [22] and IPOPT. CasADi is a toolbox which allows us to create symbolic expressions for our collocated system, which it tries to solve using IPOPT.

### D. Initialization

Due to the size and complexity of our co-design problem, we need to assist our solver by providing an initial guess for our states, inputs and our co-design parameters. There are different initialization methods with different degrees of difficulty [19], one of which is solving a simplified TO problem first. We do this by first solving rigid body dynamics, and use it to calculate actuator states using estimated co-design parameters. We use this initial guess to solve the TO problem with estimated states and co-design parameters, which is used as initial guess for the co-design problem, its implementation shown in fig. 5. The TO problems solved before our co-design problem have relaxed boundary conditions to increase solving speed, keeping into account that this approach requires the problem used as initial guess and the subsequent problem should be similar, as applying inaccurate initialization could worsen performance [23].

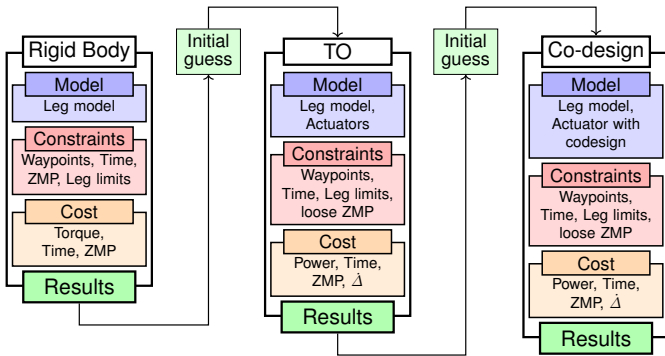


Fig. 5: Iterative approach for initial guesses for faster convergence.

## IV. RESULTS

For the following section, we first define the variables used to obtain the results. After this we give an overview of the results and visualize them. Due to the simulations providing a lot of data, we discuss our results in Section V, where we focus on the contributions of the data.

### A. Variables

1) *Leg model*: We define our leg model parameters from fig. 1 and its constraints from eq. (43) in table I. The viscous friction of the joints is set to  $d = 10^{-4}$  to represent a slight inefficiency.

TABLE I: Leg model parameters

Length [m]	Mass [kg]	Angle [rad]
$x_t = 0.4$	$m_0 = 0.5$	$-\frac{\pi}{3} < \theta_1 < \frac{\pi}{16}$
$x_h = -0.1$	$m_1 = 1.0$	$0.0001 < \theta_2 < \pi$
$l_1 = 0.5$	$m_2 = 2.0$	$-\pi < \theta_3 < \frac{\pi}{8}$
$l_2 = 0.5$	$m_3 = 2.0$	
$l_3 = 0.25$	$m_4 = 10.0$	

2) *Actuation and co-design*: We use SEA and MA, which use different motors based on the Maxon EC 90 flat 90W and the Maxon EC 22 100W respectively, which we use to define motor inertia  $I_m$  and torque constant  $\kappa_\tau$ . We define the viscous friction both types of actuation experiences as  $d = 10^{-3}$ . All SEA use the same parameters;  $n_{SEA} = 25$  and  $k_{SEA} = 1000 \text{ Nm/rad}$  and are not co-designed, as our focus is on MA design. All MA have  $n_{MA}$  and  $k_{MA}$  as co-design parameters, which are constrained by  $1 \leq n_{MA} \leq n_{max}$  and  $1 \leq k_{MA} \leq k_{max}$ . We set our upper bounds by taking a generous estimate of their maxima:  $n_{max} = 630000 \text{ m/rad}$  based on a 10mm pitch ballscrew combined with a gearing ratio of 100 and  $k_{max} = 100 \text{ kN/m}$  based on preliminary testing. Initializing of these parameters was done with an estimate based on the results from Roozing et al. [8]. We also define the pulley radii in table II, color coded to resemble fig. 3 and make the results easier to distinguish.

TABLE II: Pulley radii of Pretension Actuators

	Monoarticulated	Biarticulated
$r_{SOL} =$	$\begin{bmatrix} -0.075 \\ 0 \\ 0 \end{bmatrix}$	$r_{GAS} = \begin{bmatrix} -0.075 \\ -0.035 \\ 0 \end{bmatrix}$
$r_{VAS} =$	$\begin{bmatrix} 0 \\ 0.075 \\ 0 \end{bmatrix}$	$r_{RF} = \begin{bmatrix} 0 \\ 0.075 \\ 0.035 \end{bmatrix}$
$r_{GMAX} =$	$\begin{bmatrix} 0 \\ 0 \\ -0.075 \end{bmatrix}$	$r_{HAM} = \begin{bmatrix} 0 \\ -0.075 \\ -0.035 \end{bmatrix}$

3) *Tasks*: Figure 6 shows the initial and final conditions of each task, which define the boundary conditions set in section III-A. We constrain  $\theta_1$  and  $\theta_2$  with waypoints, but do not do so for  $\theta_3$ , done so it stabilizes the movements. We

set the initial and final states to  $\mathbf{x}(0) = \mathbf{x}(T_{\text{total}}) = 0$ , so the model starts and ends in an upright orientation. This also sets the initial pretension equal to the final pretension, so there is no energy stored in the system at start and finish. For each task we collocate 50 segments, which showed acceptable accuracy in preliminary testing. To maintain this accuracy we define  $T_{\text{max}} \leq 30$  s (42), which keeps  $dt$  within reasonable limits.

4) *Cost function and constraints:* Setting the weights changes the gradient of the cost function and was therefore done through an iterative process, adjusting after each simulation to improve results. This resulted in the following weights:  $w_{\text{Power}} = 1$ ,  $w_{\text{Time}} = 1$ ,  $w_{\Delta_{\text{SEA}}} = 10^2$ ,  $w_{\Delta_{\text{MA}}} = 1$ ,  $[w_{\text{ZMP}} = 1, \beta_{\text{ZMP}} = 10^2]$ . As constraint (44) prevents oscillating behavior, we set the lower weight for MAs to reduce the speed of storing and providing energy. The cost on ZMP was mainly decided by its slope, defined by  $\beta$ . To prevent this cost to approach infinity, it is constrained (45) by  $-0.2 \leq x_{\text{ZMP}}(t) \leq 0.5$ , to give 20% slack w.r.t the BoS. Section III-D defined two TO problems that are solved to provide an initial guess for our co-design problem. The Rigid Body TO has no actuation, so it optimizes for input torque squared, time spent and ZMP. Its ZMP is constrained by  $-0.1 \leq x_{\text{ZMP}}(t) \leq 0.4$  to force it within stable bounds. The TO without co-design is subjected to the same costs and constrained as the co-designed problem, excluding the co-design constraints (46) by removing  $\gamma$  as decision variable.

### B. Co-design parameters

The co-design results of the MAs are shown in table III, with its colors referencing fig. 3 and MA subscript referring to its configuration. The  $\text{VAS}_1$  and  $\text{VAS}_2$  and  $\text{RF}_3$  have their gearing ratio approach  $n_{\text{max}}$ , and these actuators showed practically no movement, behaving as if they were passive elastic elements. All GAS show high stiffness, comparable with aforementioned works. Upper leg biarticulation shows lower stiffness, contributed to less gravitational forces.

TABLE III: Results from co-designing MA stiffness  $k$  and gearing ratio  $n$  of configuration 1-4.

Config 1	$k$ [N/m]	$n$ [m/rad]	Config 2	$k$ [N/m]	$n$ [m/rad]
$\text{SOL}_1$	3610	12860	$\text{GAS}_2$	21570	8940
$\text{VAS}_1$	4623	$n_{\text{max}}$	$\text{VAS}_2$	5670	$n_{\text{max}}$
Config 3	$k$ [N/m]	$n$ [m/rad]	Config 4	$k$ [N/m]	$n$ [m/rad]
$\text{GAS}_3$	22400	19700	$\text{GAS}_4$	30660	5830
$\text{RF}_3$	6470	16200	$\text{RF}_4$	6160	12220
$\text{GMAX}_3$	4050	$n_{\text{max}}$	$\text{HAM}_4$	958	2640

### C. Energy and Power

Table IV shows the combined energy and mean power consumption of the SEAs, MAs and the entire configuration. The bottom row shows the total time each configuration spent, with config 0 being the fastest followed by config 2 and 1, config 3 and 4 performing worst, approaching  $T_{\text{max}}$ . Configurations with MAs show significant reductions in

energy and power consumption compared to config 0, showing that the SEAs needed to provide around 90% less average power, which results in an average total energy reduction of 80%. Out of all configurations, config 2 performs best, requiring 90% less energy. Figure 7 shows the combined

TABLE IV: Energy and mean power consumption, and time spent for configurations 0-4. Change in % is compared config 0.

		0	1	2	3	4
$E_{\text{SEA}}$	[J]	1096	225	74	88	266
			-79%	-93%	-92%	-76%
$E_{\text{MA}}$	[J]	N/A	20	41	65	142
$E_{\text{total}}$	[J]	1096	245	115	154	409
			-78%	-90%	-86%	-63%
$P_{\text{SEA, mean}}$	[W]	138.3	11.1	3.3	3.6	19.0
			-92%	-98%	-97%	-86%
$P_{\text{MA, mean}}$	[W]	N/A	0.7	1.3	1.9	4.0
$P_{\text{total, mean}}$	[W]	138.3	11.8	4.6	5.5	23.0
			-91%	-97%	-96%	-83%
$T_{\text{total}}$	[s]	12.33	24.40	21.80	29.96	29.99

power consumption over time of SEAs in the top row and MAs in the bottom row. Configurations 1, 3 and 4 all start with an extreme power peak. This is due to some MAs generating tension when the leg is at its most energy efficient position, which is then used during the movements. This is done by  $\text{SOL}_1$ ,  $\text{GAS}_3$ ,  $\text{RF}_3$ ,  $\text{RF}_4$  and  $\text{HAM}_4$ .  $P_{\text{VAS}_1}$ ,  $P_{\text{VAS}_2}$  and  $P_{\text{GMAX}_3}$  have practically no power consumption, conforming with with passive behaviour. On average, the MAs affecting the ankle ( $\text{SOL}_1$  and  $\text{GAS}_{2,3,4}$ ), consume the most power (99%, 99%, 36%, 74% of  $P_{\text{MA}_{1,2,3,4}}$  resp.), except for configuration 3 where  $P_{\text{RF}_3} = 64\%$ .

### D. Trajectory and Torques

The trajectories and applied motor torques are shown in figs. 8 and 9 respectively. As shown before, config 0 is fastest, requiring high SEA torques. Configurations 1-4 show that the MAs reduce the average SEA torques significantly, although still necessary for some movements. Configurations 1 and 2 show similar trajectories, but config 2 reaches waypoints without overshooting and requires less balancing movements like the recovery after Task 5 (9s to 14s). Configurations 3 and 4 show less efficient performance, taking their time to generate and release tension and having very rigid movement. Config 3 also shows that biarticulating the hip joint, which experiences the least gravitational torque, requires the other actuators to counter-act, meaning it could be replaced with a mono-articulated MA. Config 4 shows that the addition of antagonistic actuation increases all actuator torques without applicable benefit.

## V. DISCUSSION

In this section we first discuss our findings, afterwards we discuss the shortcomings in our methods, and what was done

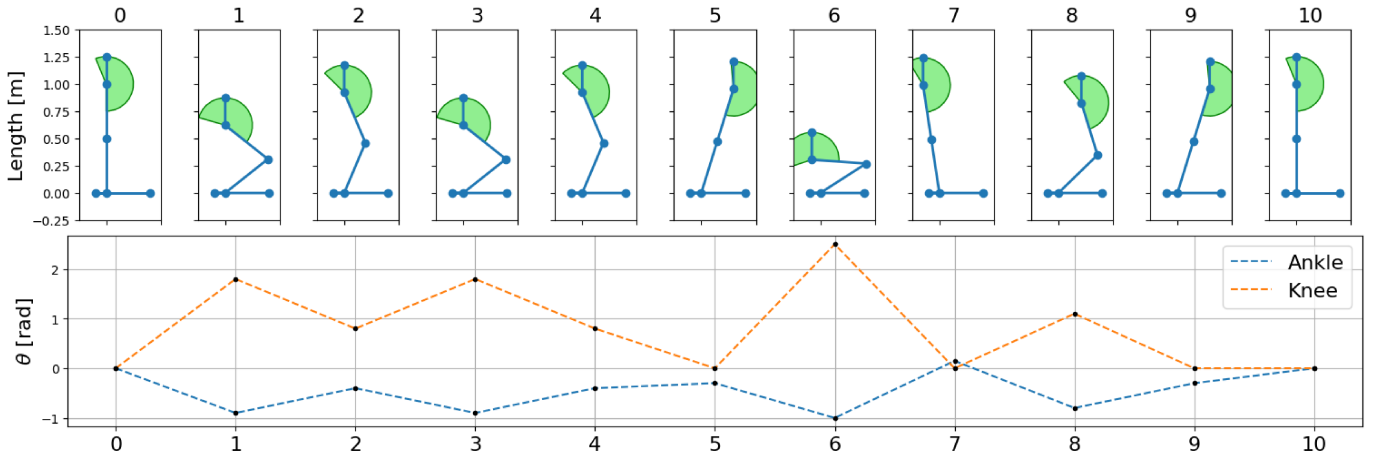


Fig. 6: Task sequence containing defined waypoints.  $\theta_1$  and  $\theta_2$  constraints are visualized as black dots, with the linear dashed line as indicator.  $\theta_3$  is free to move within the green wedge.

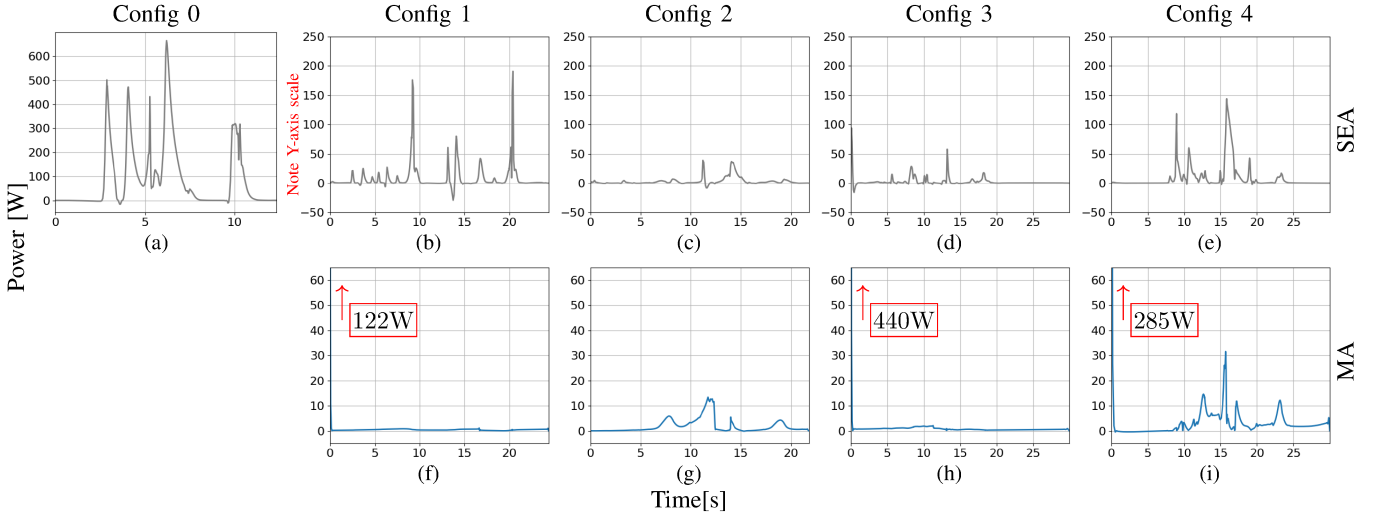


Fig. 7: Power usage grouped by SEA and MA, per configuration. Note the different x-axis for different configurations.

and could be done to alleviate them.

### A. Results

From our results we find that our co-designed configurations show significantly improved performance compared to baseline as well as an improvement between mono-articular (config 1) and biarticular (config 2), which resembles what was found in literature. Energy transfer through biarticulated actuation was found when inspecting the data, with only config 2 transferring energy from knee to ankle at 1s and 3.8s, and greater from 14s till 15.8s, where it inverts and stops at 17s. Due to the poor performance of config 3 and 4, energy transfer was not observed. The bad performance of config 3 and 4 is due to bad antagonistic pairings, as can be seen in figs. 9i, 9j, 9n and 9o, where insufficient external torque requires the model to generate its own, making it hard to move.

In the Power results we see configurations 1, 3 and 4 all have a significant peak in MA power consumption at the start

of the simulation. This behavior occurs in both mono-articular and biarticular actuators, but does not occur in configuration 2. Running the simulation from different starting points and weights did not resolve this. It is contributed to these MAs desire to start with pretension, which was tried to implement but produced no valid results.

Multiple co-designed transmission ratios converged to the maximum value, and co-designing using relaxed constraints resulted in the same passive behavior. It is assumed this is due to the defined tasks. Tasking the model to stay fixed in an orientation for some seconds should force these MAs to adjust their tensions, which was not tested but should be included for future works.

### B. Model limitations

Our model contains multiple simplifications, one of which is ignoring actuator mass in the dynamics. Due to biarticular mass distribution being an arbitrary decision and Roosting et al.

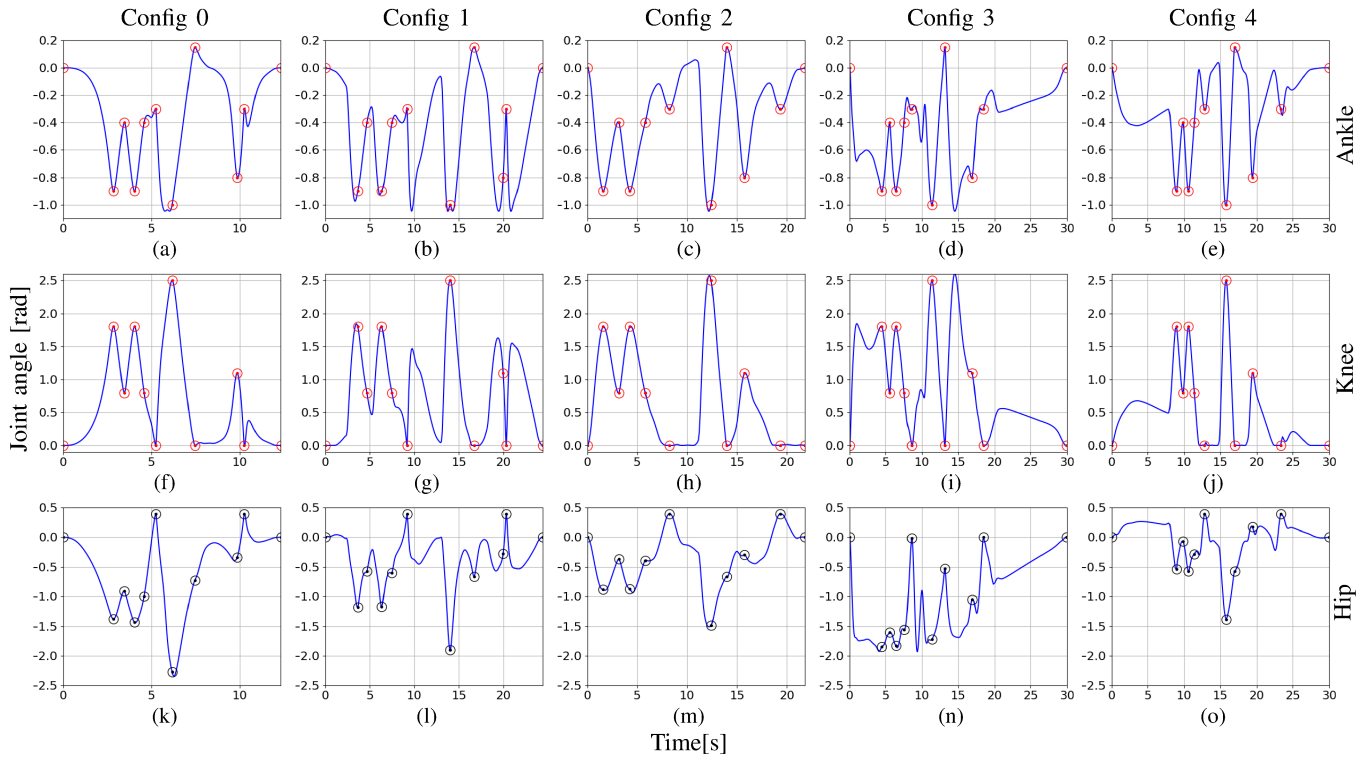


Fig. 8: Trajectories of each joint per configuration. The nodes indicate the end of task orientation, with red nodes denoting constrained waypoints. Note the different x-axis for different configurations.

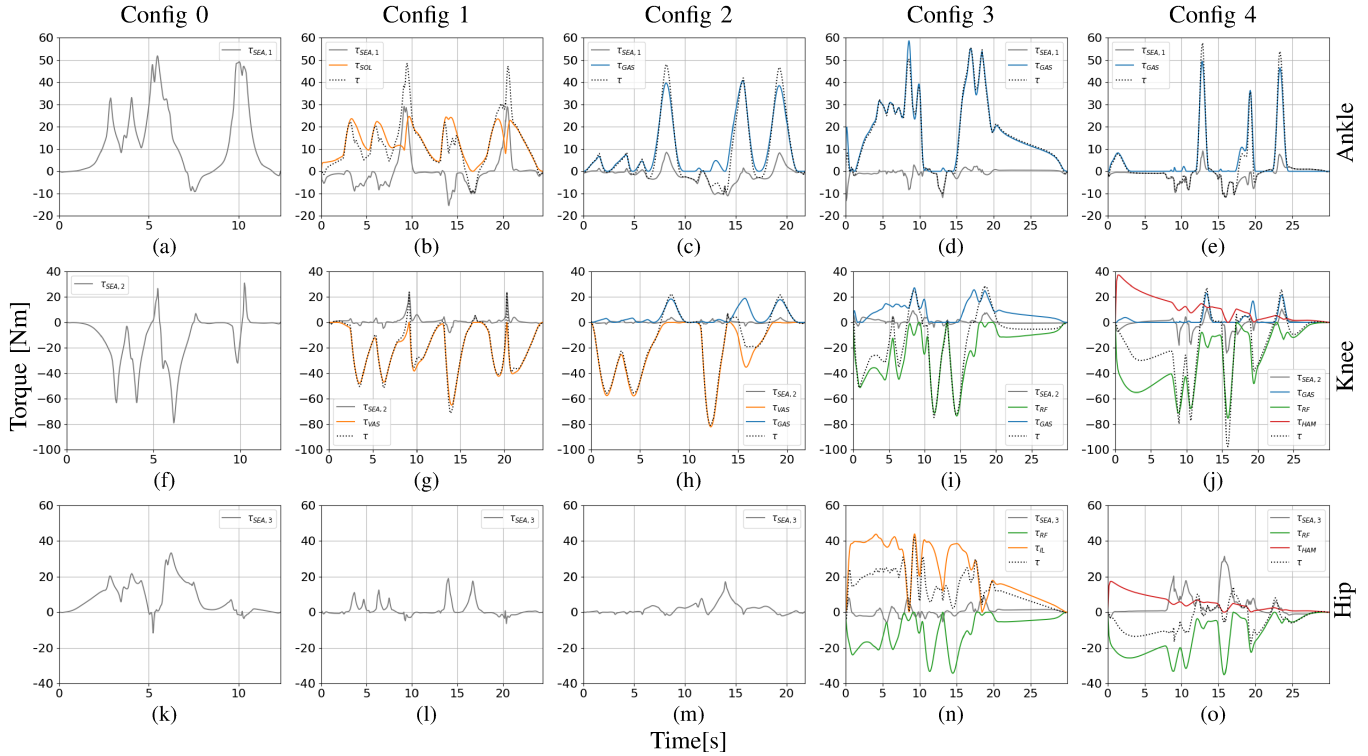


Fig. 9: Actuator torques applied to joint for each configuration. Colors reference fig. 3 colors, with grey presenting SEA torque and the dotted line presenting total torque. Note the different x-axis for different configurations.

[8] showing that weight difference between different actuation configurations makes a small enough difference to justify this simplification. Another simplification of the system is the compliance model, on which uni-directionality was enforced. This made the actuators behavior to maintain tension at all times, which explains the rigid movement of configurations 3 and 4. Allowing for slack without generating force was attempted to implement, but failed to converge.

### C. Tasking limitations

After performing less constrained simulations and different weights, it was found that the tasks were best performed by configuration 2 every time. It could mean that this set of tasks is biased towards this config. And as mentioned before, adding tasks that would have the model stay fixed in a specific orientation would show more interesting results with regards to tension control of MAs.

### D. Simulation limitations

The inclusion of the ZMP resulted in the simulations taking long periods of time. As the ZMP had to be bounded to prevent causing the solver to fail, it spent a lot more time checking the validity of each iteration. The best method to speed this up was to work with additional iterations, starting with less ZMP cost.

### E. Weights

The chosen weights for co-designing did not result in optimal results for config 3 and 4. More simulations were done setting higher  $w_{\text{Time}}$  to decrease  $T_{\text{total}}$ , which improved the  $T_{\text{total}}$  of all co-designed configurations. It also resulted in more passivity in MAs, therefore we chose for weights that resulted in more tension control.

## VI. CONCLUSION

This work has shown a method of using co-design for compliant actuators, resulting in a reduction in overall energy consumption of around 80%, approaching 90% for the most optimal configuration, and overall with SEA power requirements significantly reduced. Energy transfer was observed in the GAS, but seemed inefficient for upper leg biarticulation where gravitational torque is less. Co-designing the MAs for different configurations showed comparable co-design parameters, showing a trend that can be used for iterative design. Despite the simplifications of the problem, the results show proof-of-concept that co-design can be used for designing compliant actuation, as it resulted in similar parameters as seen in other works.

For future research we suggest using a wider array of tasks, including multiple stationary tasks to test the adjusting of tension as well as applying external forces on the model to test perturbed performance and stability of the compliant elements. Another inclusion could be optimizing mass and its distribution, which would allow optimizing of pulley radii and positioning of actuators.

## REFERENCES

- [1] A. V. Hill, "The heat of shortening and the dynamic constants of muscle," *Proceedings of the Royal Society of London. Series B - Biological Sciences*, vol. 126, no. 843, pp. 136–195, Jan. 1997, publisher: Royal Society. [Online]. Available: <https://royalsocietypublishing.org/doi/10.1098/rspb.1938.0050>
- [2] S. L. Lindstedt, T. E. Reich, P. Keim, and P. C. LaStayo, "Do muscles function as adaptable locomotor springs?" *Journal of Experimental Biology*, vol. 205, no. 15, pp. 2211–2216, Aug. 2002. [Online]. Available: <https://doi.org/10.1242/jeb.205.15.2211>
- [3] M. L. Latash, "Muscle coactivation: definitions, mechanisms, and functions," *Journal of Neurophysiology*, vol. 120, no. 1, pp. 88–104, Jul. 2018. [Online]. Available: <https://www.ncbi.nlm.nih.gov/pmc/articles/PMC6093955/>
- [4] B. I. Prilutsky and V. M. Zatsiorsky, "Tendon action of two-joint muscles: Transfer of mechanical energy between joints during jumping, landing, and running," *Journal of Biomechanics*, vol. 27, no. 1, pp. 25–34, Jan. 1994. [Online]. Available: <https://www.sciencedirect.com/science/article/pii/0021929094900299>
- [5] H. Vallery, J. Veneman, E. van Asseldonk, R. Ekkelenkamp, M. Buss, and H. van Der Kooij, "Compliant actuation of rehabilitation robots," *IEEE Robotics & Automation Magazine*, vol. 15, no. 3, pp. 60–69, Sep. 2008, conference Name: IEEE Robotics & Automation Magazine. [Online]. Available: <https://ieeexplore.ieee.org/document/4624584>
- [6] M. Hutter, C. Gehring, D. Jud, A. Lauber, C. D. Bellicoso, V. Tsounis, J. Hwangbo, K. Bodie, P. Fankhauser, M. Bloesch, R. Diethelm, S. Bachmann, A. Melzer, and M. Hoepflinger, "ANYmal - a highly mobile and dynamic quadrupedal robot," in *2016 IEEE/RSJ International Conference on Intelligent Robots and Systems (IROS)*, Oct. 2016, pp. 38–44, iSSN: 2153-0866. [Online]. Available: <https://ieeexplore.ieee.org/document/7758092>
- [7] Y. Yesilevskiy, W. Xi, and C. D. Remy, "A comparison of series and parallel elasticity in a monoped hopper," in *2015 IEEE International Conference on Robotics and Automation (ICRA)*, May 2015, pp. 1036–1041, iSSN: 1050-4729. [Online]. Available: <https://ieeexplore.ieee.org/document/7139304>
- [8] W. Roozing, Z. Ren, and N. G. Tsagarakis, "An efficient leg with series-parallel and biarticular compliant actuation: design optimization, modeling, and control of the eLeg," *The International Journal of Robotics Research*, vol. 40, no. 1, pp. 37–54, Jan. 2021, publisher: SAGE Publications Ltd STM. [Online]. Available: <https://doi.org/10.1177/0278364919893762>
- [9] F. Ruppert and A. Badri-Spröwitz, "Series Elastic Behavior of Biarticular Muscle-Tendon Structure in a Robotic Leg," *Frontiers in Neurobotics*, vol. 13, 2019. [Online]. Available: <https://www.frontiersin.org/articles/10.3389/fnbot.2019.00064>
- [10] K. Junius, M. Moltedo, P. Cherule, C. Rodriguez-Guerrero, B. Vanderborght, and D. Lefeber, "Biarticular elements as a contributor to energy efficiency: biomechanical review and application in bio-inspired robotics," *Bioinspiration & Biomimetics*, vol. 12, no. 6, p. 061001, Nov. 2017, publisher: IOP Publishing. [Online]. Available: <https://dx.doi.org/10.1088/1748-3190/aa806e>
- [11] N. Zakaryan, M. Harutyunyan, and Y. Sargsyan, "Conceptual Mechanical Design and Control of Novel Human Spine Inspired Multi-articular Robotic Manipulators," in *Advances in Mechanism and Machine Science*, M. Okada, Ed. Cham: Springer Nature Switzerland, 2023, pp. 448–457.
- [12] J. Lee, G. Lee, S. Hong, S. Lee, J. H. Kim, and Y. Oh, "A novel multi-articular leg mechanism for biped robots inspired by bi-articular muscle," in *2016 6th IEEE International Conference on Biomedical Robotics and Biomechanics (BioRob)*, Jun. 2016, pp. 1372–1377, iSSN: 2155-1782. [Online]. Available: <https://ieeexplore.ieee.org/document/7523825>
- [13] W. Roozing, Z. Li, G. A. Medrano-Cerda, D. G. Caldwell, and N. G. Tsagarakis, "Development and Control of a Compliant Asymmetric Antagonistic Actuator for Energy Efficient Mobility," *IEEE/ASME Transactions on Mechatronics*, vol. 21, no. 2, pp. 1080–1091, Apr. 2016, conference Name: IEEE/ASME Transactions on Mechatronics. [Online]. Available: <https://ieeexplore.ieee.org/document/7303955>
- [14] G. Fadini, "A versatile co-design framework for simultaneous optimization of robots' hardware and control."
- [15] G. Bravo-Palacios, A. D. Prete, and P. M. Wensing, "One Robot for Many Tasks: Versatile Co-Design Through Stochastic Programming," *IEEE Robotics and Automation Letters*, vol. 5, no. 2, pp. 1680–1687,

- Apr. 2020, conference Name: IEEE Robotics and Automation Letters. [Online]. Available: <https://ieeexplore.ieee.org/document/8972465>
- [16] T. Dinev, C. Mastalli, V. Ivan, S. Tonneau, and S. Vijayakumar, "A Versatile Co-Design Approach For Dynamic Legged Robots," Jul. 2022, arXiv:2103.04660 [cs]. [Online]. Available: <http://arxiv.org/abs/2103.04660>
- [17] W. Roozing, Z. Li, D. G. Caldwell, and N. G. Tsagarakis, "Design Optimisation and Control of Compliant Actuation Arrangements in Articulated Robots for Improved Energy Efficiency," *IEEE Robotics and Automation Letters*, vol. 1, no. 2, pp. 1110–1117, Jul. 2016, conference Name: IEEE Robotics and Automation Letters. [Online]. Available: <https://ieeexplore.ieee.org/document/7393471>
- [18] W. Roozing, "Modeling and Control of Adjustable Articulated Parallel Compliant Actuation Arrangements in Articulated Robots," *Frontiers in Robotics and AI*, vol. 5, 2018. [Online]. Available: <https://www.frontiersin.org/articles/10.3389/frobt.2018.00004>
- [19] M. Kelly, "An Introduction to Trajectory Optimization: How to Do Your Own Direct Collocation," *SIAM Review*, vol. 59, no. 4, pp. 849–904, Jan. 2017, publisher: Society for Industrial and Applied Mathematics. [Online]. Available: <https://epubs.siam.org/doi/10.1137/16M1062569>
- [20] S. Kajita and B. Espiau, "Legged Robots," in *Springer Handbook of Robotics*, B. Siciliano and O. Khatib, Eds. Berlin, Heidelberg: Springer Berlin Heidelberg, 2008, pp. 361–389. [Online]. Available: [https://doi.org/10.1007/978-3-540-30301-5\\_17](https://doi.org/10.1007/978-3-540-30301-5_17)
- [21] S. Moreno-Martín, L. Ros, and E. Celaya, "Collocation methods for second and higher order systems," *Autonomous Robots*, vol. 48, no. 1, p. 2, Jan. 2024. [Online]. Available: <https://doi.org/10.1007/s10514-023-10155-z>
- [22] J. A. E. Andersson, J. Gillis, G. Horn, J. B. Rawlings, and M. Diehl, "CasADI: a software framework for nonlinear optimization and optimal control," *Mathematical Programming Computation*, vol. 11, no. 1, pp. 1–36, Mar. 2019. [Online]. Available: <https://doi.org/10.1007/s12532-018-0139-4>
- [23] E. A. Yildirim and S. J. Wright, "Warm-Start Strategies in Interior-Point Methods for Linear Programming," *SIAM Journal on Optimization*, vol. 12, no. 3, pp. 782–810, Jan. 2002. [Online]. Available: <http://epubs.siam.org/doi/10.1137/S1052623400369235>